CFSRC COLLOQUIUM

Proceedings of the Cold-Formed Steel Research Consortium Colloquium
20-22 October 2020 (cfsrc.org)

Topology Optimization of Cold-Formed Steel Deck Diaphragms with Irregularities

Astrid W. Fischer[1], James K. Guest[2], Benjamin W. Schafer[3]

Abstract

The objective of this paper is to explore the optimization of building roofs composed of bare cold-formed steel deck profiles when subjected to lateral demands such that the diaphragm response dominates the roof design considerations. Through variation in the deck profile, deck thickness, sidelap connectors, and structural connectors the in-plane shear stiffness and strength, that may be realized by a bare steel deck acting as a diaphragm, covers a significant range. In addition, although deck orientation is not typically varied within a roof – the profiled nature of a steel deck provides starkly different in-plane rigidities along and across the deck profile. Here we consider the application of topology optimization to aid in determining an optimal layout for a cold-formed steel deck roof. The topology optimization problem is formulated employing planar orthotropic elements for the roof deck and seeks to determine the maximum stiffness (i.e. minimum compliance) under an equivalent static in-plane lateral load subject to constraints. Constraints are placed on the basic roof element properties that are consistent with ranges of available deck and connections. The optimizer considers thickness of the planar elements, in essence a proxy for in-plane stiffness, and orientation of the planar elements. Conversion of the optimization results into a realizable steel deck roof is demonstrated. A series of examples are considered, including a rectangular roof, as well as plan irregularities including non-rectangular building shape, and roof cutouts. Significant future challenges remain and are briefly enumerated.

1. Introduction

All buildings are built with a vertical lateral force resisting system (vLFRS) in the form of shear walls, moment frames or braced frames, as illustrated in Figure 1 with red braces. The horizontal lateral force resisting system (hLFRS), e.g. a floor diaphragm, transfers the lateral loads horizontally to the vLFRS. Traditionally, floor diaphragms are designed such that the chords and collectors transfer loads at the boundary to the VLFRS, and the diaphragm deck is designed to resist the in-plane shear forces and gravity loads. Steel deck diaphragms can be both bare and composite, but are essentially highly orthotropic either way due to the corrugated steel sheet, which in one direction equals the strength and stiffness of the steel sheet, but in the direction perpendicular to the folds has stiffness equal to folding or stretching of the corrugated sheet. Usually, diaphragm decks are placed with the same orientation across the diaphragm, however, using the orthotropic behavior to design a diaphragm, where each deck plate can be oriented independently, the diaphragm behavior can be maximized, and chords and collectors can potentially be integrated into the diaphragm design itself.

Diaphragms can be designed for maximum stiffness through topology optimization by selection of appropriate deck types and deck orientation for small segments of the diaphragm. This will ensure a better path for transferring loads to the vLFRS, e.g. braced frames. In the following, the floor layouts are optimized using the gradient-based solver Method for Moving Asymptotes (MMA) [1].

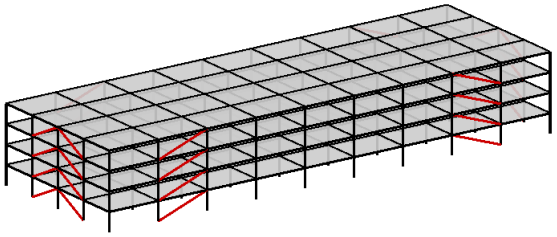

Figure 1: SDII building archetype with BRB braced frames [2]

[1] Graduate Candidate, Johns Hopkins University Civil and Systems Engineering Department, Baltimore, Maryland, winther@jhu.edu
[2] Associate Professor, Johns Hopkins University Civil and Systems Engineering Department, Baltimore, Maryland, jkguest@jhu.edu
[3] Professor, Johns Hopkins University Civil and Systems Engineering Department, Baltimore, Maryland, schafer@jhu.edu

2. Topology Optimization Formulation

Bare steel deck diaphragms are designed with maximum stiffness as the objective, which is equivalent to the minimum compliance, or minimum external work formulation [3].

$$\min_{\phi\ \psi} f = \mathbf{F}^T\ \mathbf{d} \tag{1}$$

The formulation is extended to include two load cases, for loads in two perpendicular directions, that will result in independent load paths for the two loading cases:

$$\min_{\phi\ \psi} f = \mathbf{F}_1^T\ \mathbf{d}_1 + \ \mathbf{F}_2^T\ \mathbf{d}_2 \tag{2}$$

The objective function is subject to static equilibrium conditions of the system and an upper bound of available material:

$$s.t. \quad \mathbf{K}\ \mathbf{d}_i - \mathbf{F}_i = \mathbf{0} \tag{3}$$

$$\sum_{e\in\Omega} \rho^e\ v^e - V \leq 0 \tag{4}$$

Where $\mathbf{F}_i$ is the applied load vector for load case i, $\mathbf{d}_i$ denotes the nodal displacements for load case i, and the global stiffness matrix $\mathbf{K}$ is assembled from element stiffness matrices $\mathbf{K}^e$. v^e denotes the element volume, and the available volume of material in the design domain is denoted V.

Variables ϕ^e and ψ^e are design variables, and are mapped to the material concentration, ρ^e, and the material orientation, θ^e, in element e, through a weighted average [4] [5]:

$$\rho^e = \frac{\sum_{i\in N^e}\ \phi_i \mathrm{w}(\mathrm{x}_i - \mathrm{x}^e)}{\sum_{i\in N^e} \mathrm{w}(\mathrm{x}_i - \mathrm{x}^e)} \tag{5}$$

$$\theta^e = \frac{\sum_{i\in N^e}\ \psi_i \mathrm{w}(\mathrm{x}_i - \mathrm{x}^e)}{\sum_{i\in N^e} \mathrm{w}(\mathrm{x}_i - \mathrm{x}^e)} \tag{6}$$

Where $w(x_i - x^e)$ is a linear weighting function that assigns the closet design variables with the largest weights:

$$w(x_i - x^e) = \begin{Bmatrix} \frac{r_{min} - \|x_i - x^e\|}{r_{min}} & \text{if } \ i \in N^e \\ 0 & \text{otherwise} \end{Bmatrix} \tag{7}$$

N^e is a set of elements within a radius of r_{min} of element e:

$$i \in N^e \quad if \quad \|x_i - x^e\| \leq r_{min} \tag{8}$$

The material concentration, ρ^e, and the material orientation, θ^e, are subject to upper and lower limits:

$$\rho_{min} \leq \rho^e \leq\ 1 \quad \forall\ e \in \Omega \tag{9}$$

$$-\frac{\pi}{2} \leq \theta^e \leq \frac{\pi}{2} \quad \forall\ e \in \Omega \tag{10}$$

The deck system is treated as a 2D continuum domain and is discretized using rectangular four node plane stress elements and the element stiffness matrices $\mathbf{K}^e$ is defined as:

$$\mathbf{K}^e(\rho^e\ , \theta^e) = \rho^e\ \int_{\Omega^\mathrm{e}} \mathbf{B}^{eT} \mathbf{D}^e(\theta^e)\ \mathbf{B}^e\ d\Omega^\mathrm{e} \tag{11}$$

In which $\mathbf{B}^e$ is the strain-displacement matrix, the element volume domain is denoted Ω^e, and $\mathbf{D}^e$ denotes the element constitutive stiffness matrix, rotated by angle θ^e.

$$\mathbf{D}^e(\theta^e) = \ \mathbf{R}(\theta^e)^T\ \mathbf{D}_0{}^e\ \mathbf{R}(\theta^e) \tag{12}$$

2.1 Sensitivities

The MMA [1] optimizer is adopted herein and is a gradient based optimizer that requires the gradients of the objective function and constraints to be computed with respect to the independent design variables ϕ and ψ. The derivatives of the displacements show up in the sensitivities of the objective function and can be eliminated with the use of the adjoint method [6], resulting in the simple sensitivity expressions:

$$\frac{\partial f}{\partial \rho^i} = \sum_{i=1}^{2} - \mathbf{d}_i^{eT}\ \frac{\partial \mathbf{K}^e}{\partial \rho^i}(\rho^e\ , \theta^e)\ \mathbf{d}_i^e \tag{13}$$

$$\frac{\partial f}{\partial \theta^i} = \ \sum_{i=1}^{2} - \mathbf{d}_i^{eT}\ \frac{\partial \mathbf{K}^e}{\partial \theta^i}(\rho^e\ , \theta^e)\ \mathbf{d}_i^e \tag{14}$$

Where the element stiffness derivatives with respect to the material density ρ and material orientation θ are:

$$\frac{\partial \mathbf{K}^e}{\partial \rho^i}(\rho^e\ , \theta^e) = \frac{\partial \rho^e}{\partial \rho^i} \int_{\Omega^\mathrm{e}} \mathbf{B}^{eT} \mathbf{D}^e(\theta^e)\ \mathbf{B}^e\ d\Omega^\mathrm{e} \tag{15}$$

$$\frac{\partial \mathbf{K}^e}{\partial \theta^i}(\rho^e\ , \theta^e) = \rho^e\ \int_{\Omega^\mathrm{e}} \mathbf{B}^{eT} \frac{\partial \mathbf{D}^e}{\partial \theta^i}(\theta^e)\ \mathbf{B}^e\ d\Omega^\mathrm{e} \tag{16}$$

The derivative of the constitutive stiffness matrix:

$$\frac{\partial \mathbf{D}^e}{\partial \rho^i}(\theta^e) = \ \mathbf{R}(\theta^e)^T \frac{\partial \mathbf{D}_\mathbf{0}^e}{\partial \rho^i} \mathbf{R}(\theta^e)\ \mathbf{0} \tag{17}$$

$$\frac{\partial \mathbf{D}^e}{\partial \theta^i}(\theta^e) = \frac{\partial \mathbf{R}(\theta^e)^T}{\partial \theta^i}\ \mathbf{D}_0{}^e\ \mathbf{R}(\theta^e)\ +\ \mathbf{R}(\theta^e)^T \mathbf{D}_0{}^e\ \frac{\partial \mathbf{R}(\theta^e)}{\partial \theta^i} \tag{18}$$

Lastly, the material density and material orientation derivatives with respect to the design variables, ϕ and ψ, are defined:

$$\frac{\partial \theta^e}{\partial \psi_i} = \frac{\partial \rho^e}{\partial \phi_i} = \frac{w(x_i - x^e)}{\sum_{i\in N^e}\ w(x_i - x^e)} \tag{19}$$

2.2 Diaphragm Stiffness Properties

Bare steel deck diaphragms are designed by shear strength and stiffness according to AISI S310 [7], which provides formulas developed and recommended for corrugated steel decks. Bare steel deck diaphragms are composed of many corrugated steel plates, that are attached together with sidelap fasteners along edges and the decks are secured to the underlying structure with structural fasteners. Variations of the corrugations, plate thickness, fastener type, and spacing all have an impact on the strength and stiffness of the deck. DDM04 [8] provides extensive strength tables with over 65,000 different deck configurations for use in design.

Xia and Friswell's method [9] for highly orthotropic corrugated plates are used to find Young's moduli for the steel decks alongside the formulas in AISI S310 for shear strength and stiffness. An approximation of the tabled strength and stiffness values as a linear function of variable ϱ is illustrated in Figure 2. The Young's modulus parallel to the corrugations, E_1', is the strong axis of deck, while E_2' is the weak axis, G' is the shear stiffness and V is the shear strength of the deck.

$$G' = \frac{\varrho}{\varrho_{max}} G'_{max} \tag{20}$$

$$E_1' = \frac{\varrho}{\varrho_{max}} E_{1\,max} \tag{21}$$

$$E_2' = \frac{\varrho}{\varrho_{max}} E_{2\,max} \tag{22}$$

$$V = \frac{\varrho}{\varrho_{max}} V_{max} \tag{23}$$

ϱ is determined as a function of corrugation layout, plate thickness, faster strengths and fastener spacing for both structural and sidelap connections:

$$\varrho = \frac{s}{d}\frac{t}{t_{max}}\frac{L_{max}}{L}\left(\frac{Pnf}{Pnf_{max}}\right)^{1/4}\frac{Ls_{max}}{Ls}\left(\frac{Pns}{Pns_{max}}\right)^{1/4} \tag{24}$$

Where s/d is the total corrugation length over the width of one corrugation, L is the span of the deck and L_s is the sidelap fastener spacing. P_{nf} and P_{ns} is the strength of structural and sidelap fasteners, respectively.

The design variable for the material density, $\rho \in [0,1]$, is related to ϱ through:

$$\varrho = \varrho_{min} + (\varrho_{max} - \varrho_{min})\rho \tag{25}$$

The upper and lower bounds of the bare steel deck diaphragm stiffnesses are listed in Table 1; notice in particular the large difference between the *E₁'* and *E₂'* stiffness (prime signifies stiffness times the plate thickness), but also the large shear stiffness range.

Table 1: Extreme values for the diaphragm Young's moduli and shear stiffness

		min	max
G'	[MN/m]	0.94	42.23
	(kip/in)	*5.38*	*241.12*
E_1'	[MN/m]	112.92	505.22
	(kip/in)	*644.76*	*2884.90*
E_2'	[kN/m]	4.62	156.69
	(kip/in)	*0.026*	*0.90*
ϱ	[-]	0.15	2.90

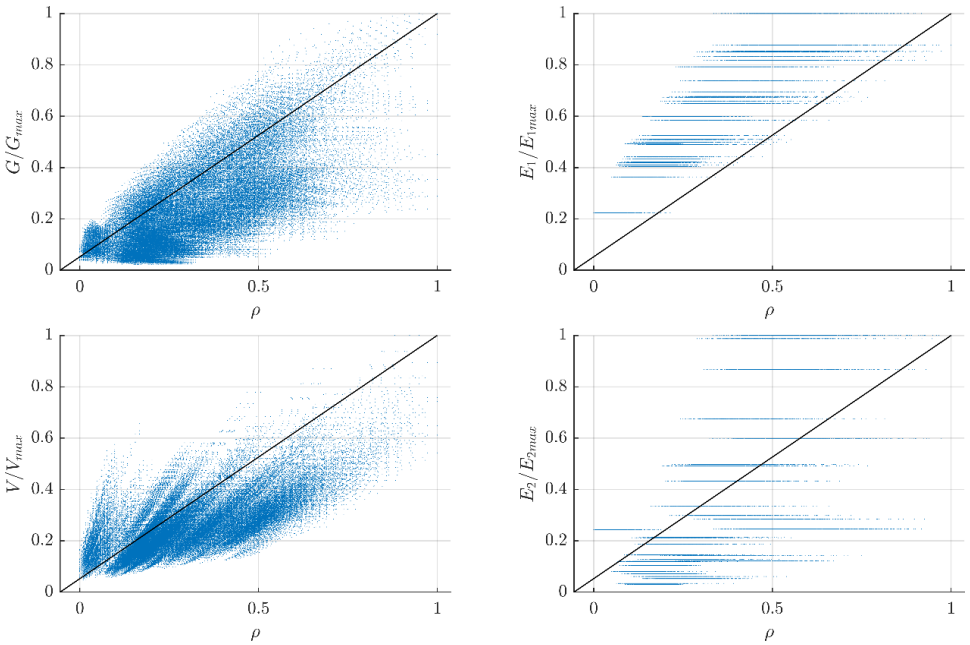

Figure 2: Shear stiffness, axial stiffnesses and shear strength variation with design variable ρ.

3. Diaphragm Examples

Four different diaphragm examples will be optimized for maximum stiffness using the minimum compliance formulation in Equations 2-19. For the optimization analyses, a volume fraction of $V = 50\%$, which corresponds to a uniform diaphragm design, are used across the examples. The initial values for the design variables are an even distribution of material $\phi = \rho = 0.5$ and material orientation $\psi = \theta = 0$ in all elements.

The diaphragms have dimensions $h = 30.48m\ (100\ ft)$, $W = 45.72m\ (150ft)$ and $L = 91.44m\ (300ft)$ and are subjected to a distributed load in two perpendicular directions, representing inertia forces, with magnitude based on the tributary area of the diaphragm. The load in each direction sums up to $P_i = 1186\ kN\ (267\ kips)$ for the rectangular diaphragms and $P_i = 1324\ kN\ (298\ kips)$ for the organic shaped diaphragm:

$$P_1 = \sum p_1 \tag{26}$$

$$P_2 = \sum p_2 \tag{27}$$

The lateral supports of the diaphragms are at the locations of the vertical lateral force resistance systems (vLFRS) and the supports can only resist loads in the direction of the vLFRS plane. Finally, the material properties are defined in Equations 20-25 for use in the optimization.

Three diaphragm designs are presented for each diaphragm example: One design is based on the traditional design method assigning deck type based on the shear demand across the diaphragm, the deck orientation is constant with $\theta = 0$. An optimized design based on the formulation of Equations 2-19, and an interpreted design, that is based on the freely optimized design, which have segments with the same deck type and orientation, making it a more realistic possible construction. The material density (ρ) and deck orientation (θ) is defined inside a segment to equal the average values. A segment is defined such that least change is made to the freely optimized design.

3.1 Example - SDII Archetype

Inspired by the archetype building model for the SDII project [2] in Figure 1 the diaphragm in Figure 3a is developed with supports at the location of the braced frames and uniform distributed loads on all sides. The design in Figure 3b is based on the traditional design approach, designing for a shear demand across the diaphragm and assigning a deck type to each section. The shades of grey indicate the deck type in terms of the ρ value, with white being $\rho = 0$ (minimum stiffness, $\varrho = 0.15$) and black for $\rho = 1$ (maximum stiffness, $\varrho = 2.90$). A volume fraction of $V = 50\%$ is upheld for this design.

The optimized design layout in Figure 3c, is illustrated with grey shades for the material density ρ and for each element the material orientation, θ^e, is depicted as a short red line in the E_1 (strong) direction. The optimized design has some features worth noting: there are high stiffness deck types along the long sides of the diaphragm, indicating the need for chords. Collectors along the short sides that transfer forces from the chords to the supports are also indicated. In addition to traditional design of chords and collectors, there are struts from corners to the center of the diaphragm.

Based on the optimized design an interpretation of the design is made in Figure 3d, maintaining a volume fraction of $V = 50\%$. The collector and struts are preserved in the interpreted design, while chords are not present in that design.

Comparing the objective function (Equation 2) for the different design layouts gives a measurable performance for the designs, see Table 2, where smaller function values indicate a better design. Choosing the optimized design (Figure 3c) above the traditional design (Figure 3b) will result in 54 times stiffer diaphragm behavior, without utilizing more material, with the applied loads used in this analysis. Choosing the interpreted design (Figure 3d) above the optimized design leads to 4 times more flexible diaphragm behavior, that is still 14 times stiffer than the traditional design with the same amount of material

Table 2: Objective function values for the diaphragm design examples

		Optimized design	Traditional design	Interpreted design
SDII	[kN m]	64	3447	243
	[kips ft]	*47*	*2542*	*179*
SDII with cutout	[kN m]	104	4274	459
	[kips ft]	*77*	*3152*	*338*
Organic perimeter	[kN m]	171	10602	704
	[kips ft]	*126*	*7818*	*519*
Organic internal	[kN m]	58	5080	522
	[kips ft]	*43*	*3747*	*385*

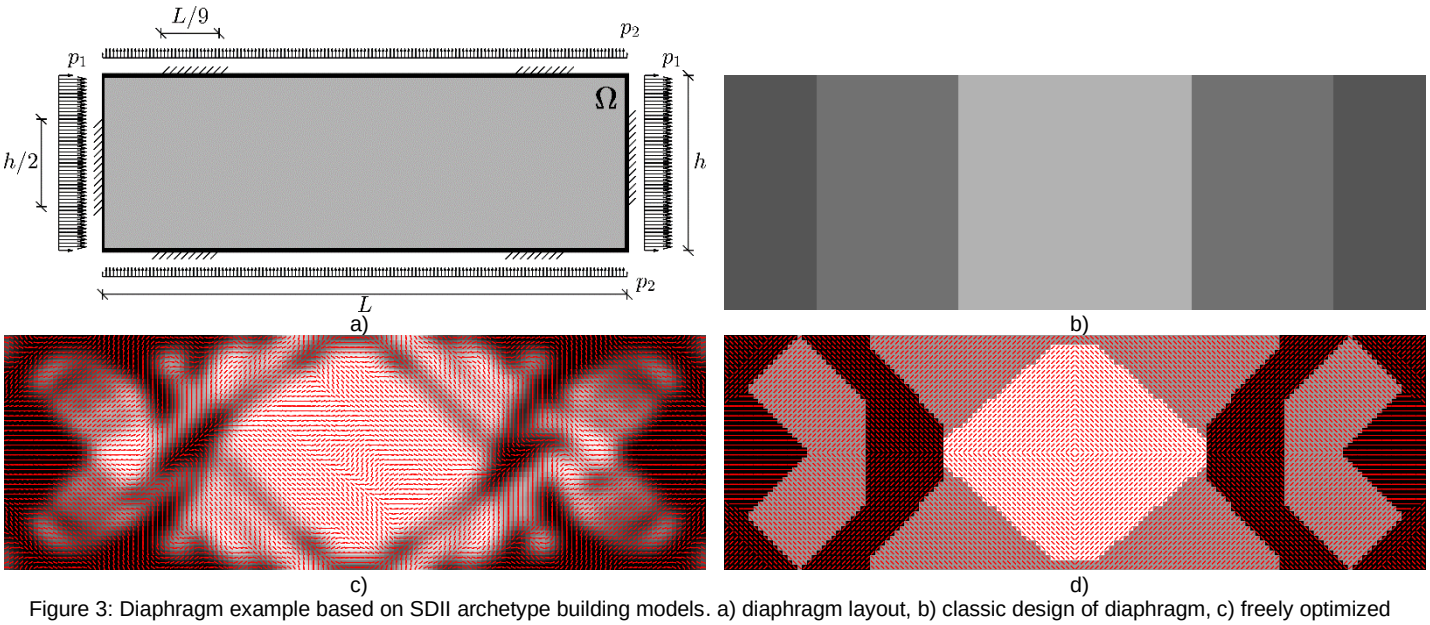

Figure 3: Diaphragm example based on SDII archetype building models. a) diaphragm layout, b) classic design of diaphragm, c) freely optimized diaphragm, and d) interpreted optimized diaphragm design.

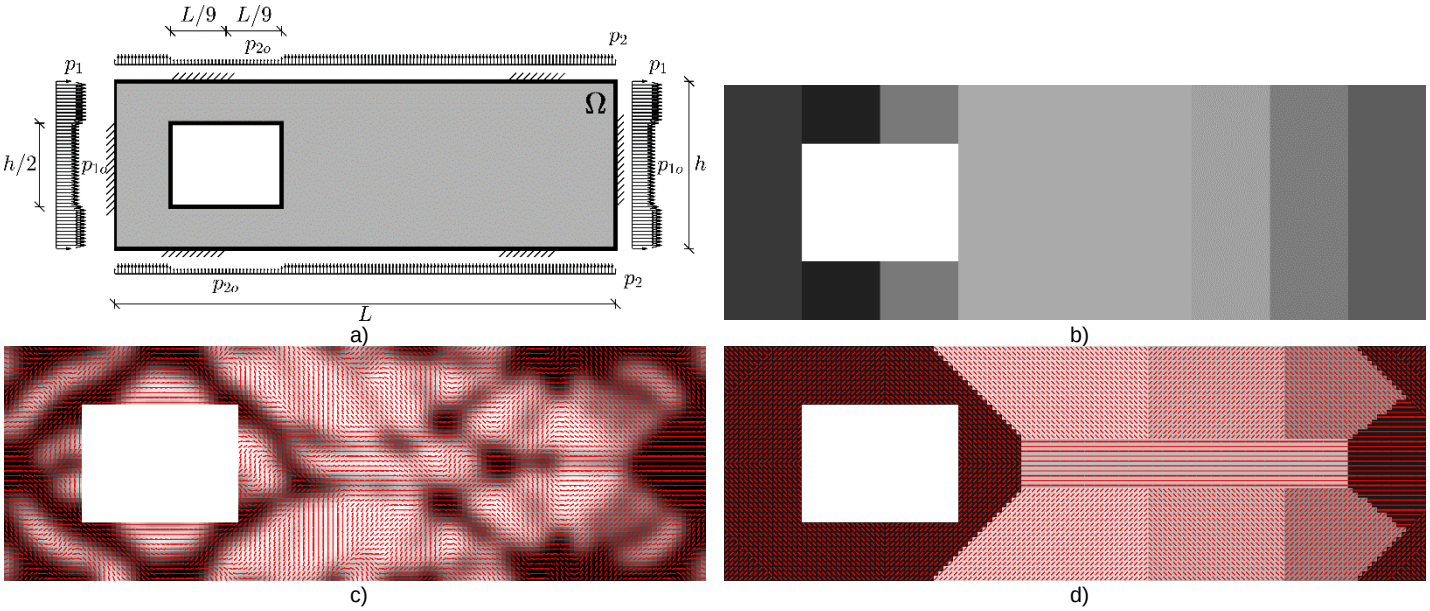

Figure 4: Diaphragm example based on SDII archetype building models with cutout. a) diaphragm layout, b) classic design of diaphragm, c) freely optimized diaphragm, and d) interpreted optimized diaphragm design.

3.2 Example – SDII Archetype with Cutout

Figure 4a is the SDII archetype example modified to now include an opening/cut-out in the diaphragm. The location of the opening is based on the bay spacing for the gravity system and could be interpreted as an atrium or other large opening. The cutout location does interfere with the strut structure indicated in Figure 3c for the solution without a cutout.

The traditional design in Figure 4b has a higher deck stiffness around the cutout to accommodate the larger shear stresses caused by the cutout. To maintain a 50% “volume fraction” a lower deck stiffness is chosen for the rest of the diaphragm, compared to Figure 3b.

The optimized design (Figure 4c) has similarities with the optimized design in Figure 3c with indication of a chord along the long sides of the diaphragm and collectors at the ends. The end away from the cutout has struts from the

corners to the center of the diaphragm similar to the ones in Figure 3c. The cutout results in struts all around the cutout to transfer forces from the chord to the support.

The interpreted design in Figure 4d is reinforcing the cutout with stiff deck types orienting at 45 ° around the cutout and with a stiffer collector at the end away from the cutout. In between, low stiffness deck types are chosen with orientation beneficial to the diaphragm. This design is 4 times less stiff than the more complex optimized design (Figure 4c) but 9 times stiffer than the traditional design (Figure 4b).

3.3 Example – Organic Shape with Perimeter Supports

An organic plan shaped building is subjected to investigation, to see how the deck placement and orientation can improve the overall stiffness of the diaphragm and explore the application of the methodology to more complex geometries. The lateral supports are located on the perimeter of this diaphragm, see Figure 5a, and the load is a function of the depth/width of the diaphragm.

Visible in all three design layouts, traditional (Figure 5b), optimized (Figure 5c), and interpreted (Figure 5d) is a high demand for stiffness and strength along the entire perimeter. For the optimized and the interpreted designs, transfer "beams" are crossing the middle of the diaphragm. The optimized design is about 62 times stiffer than the traditional design and the interpreted design is about 15 times more stiff than the traditional design.

3.4 Example – Organic Shape with Internal Supports

Figure 6a illustrates the same organic shape with internal lateral supports for the diaphragm. The change of support locations changes the optimized design considerably from Figure 5c to Figure 6c. The optimized design in Figure 6c demands more stiffness near the internal supports and less stiffness at boundary, this feature is preserved in the interpreted design in Figure 6d.

The traditional design in Figure 6b has a low shear demand cross the domain due to the location of the supports, this results in an almost uniform design with highest demands at the support locations. The interpreted design is about 10 times stiffer than the traditional design in Figure 6b. The optimized design is about 88 times more stiff than the traditional design.

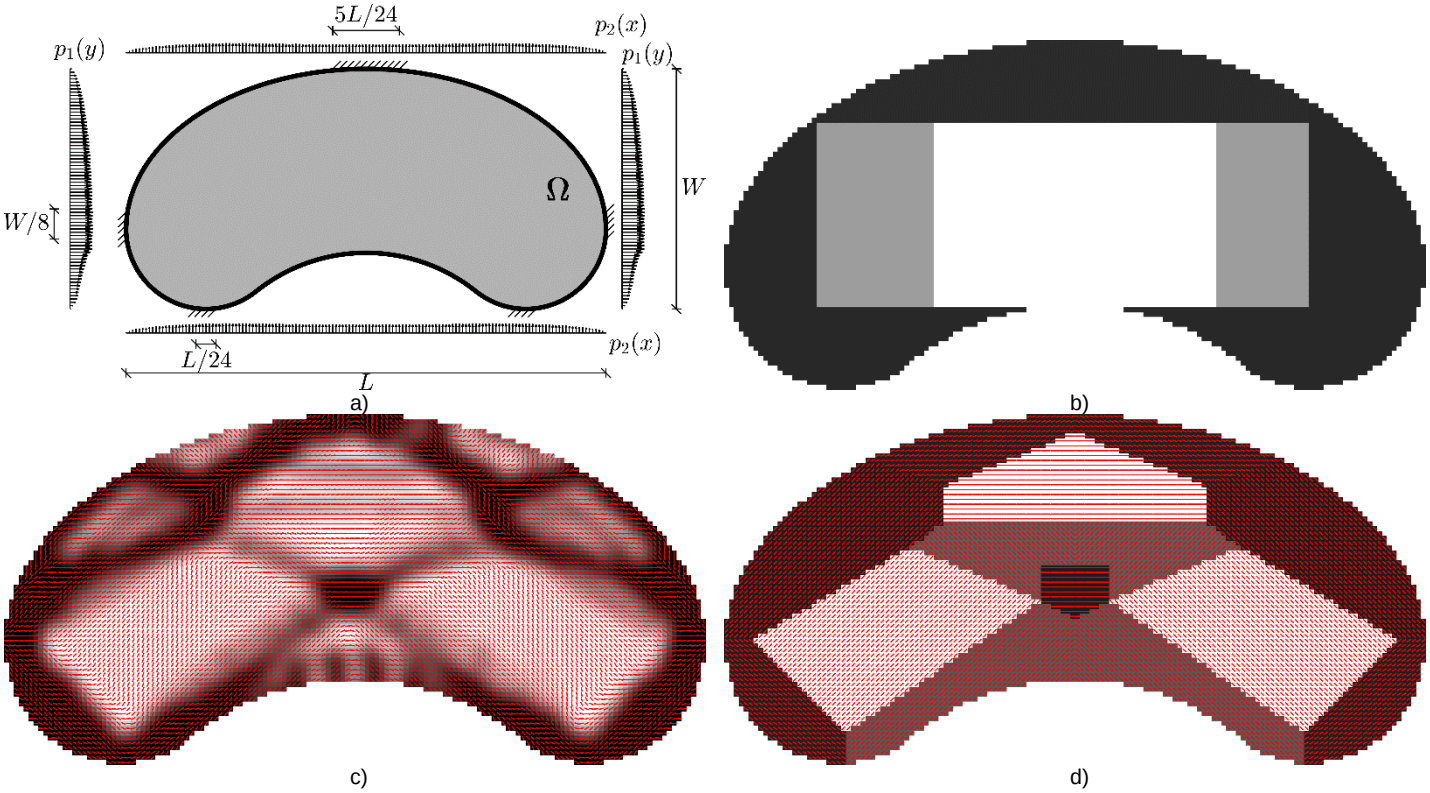

Figure 5: Diaphragm example based on an organic shape with supports at the boundary. a) diaphragm layout, b) classic design of diaphragm, c) freely optimized diaphragm, and d) interpreted optimized diaphragm design.

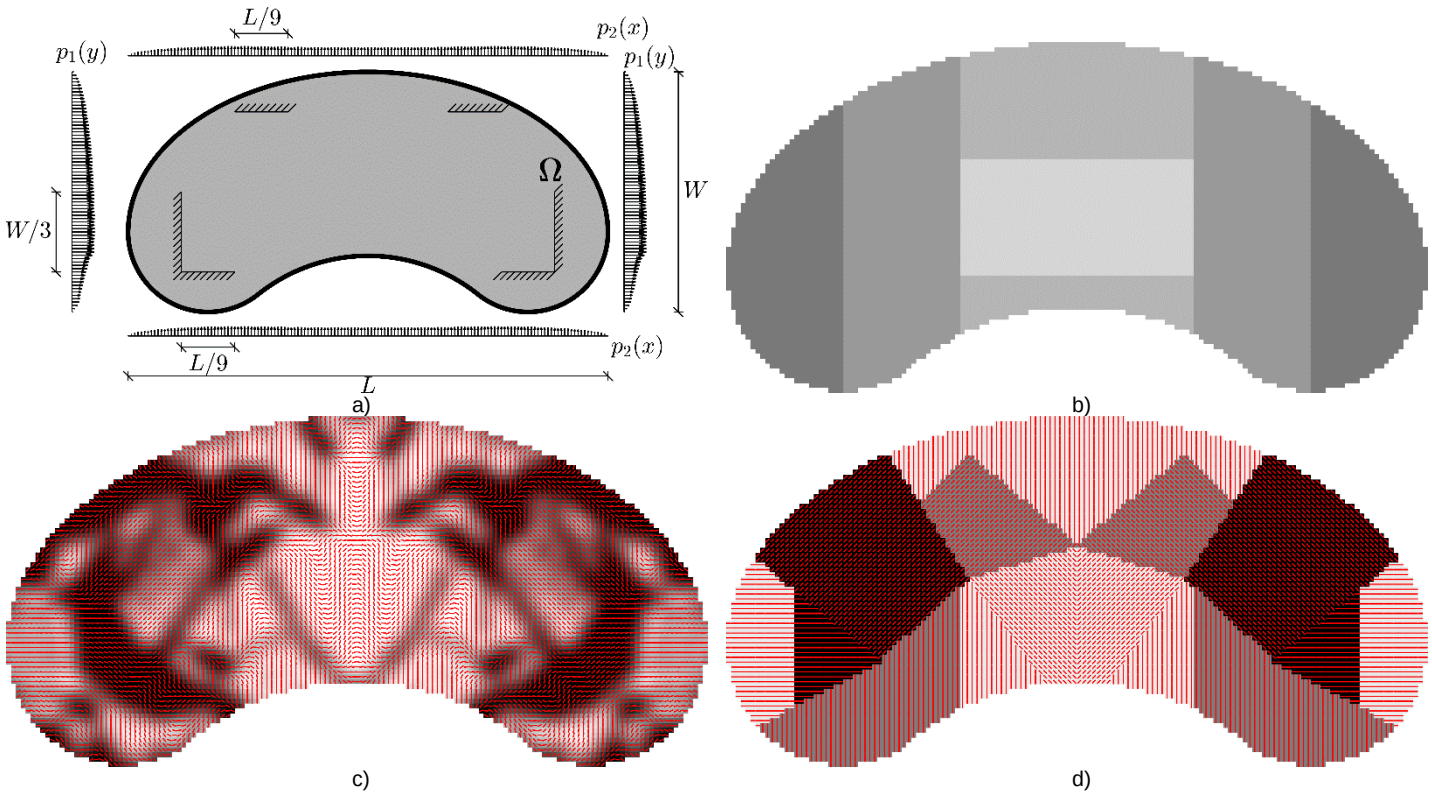

Figure 6: Diaphragm example based on an organic shape with internal supports. a) diaphragm layout, b) classic design of diaphragm, c) freely optimized diaphragm, and d) interpreted optimized diaphragm design.

5. Conclusions

The highly orthotropic behavior of corrugated steel decks and interest in improving the diaphragm design has motivated the work to develop a two-dimensional topology optimization algorithm that uses the material orientation and material stiffness as design variables. Four different diaphragm layouts, including cutouts and organic shaped diaphragms, are subjected to a distributed load along the boundary, representing inertia forces, that acts in both horizontal directions. The diaphragms are optimized for maximum stiffness considering both load directions. The freely optimized designs are subjected to interpretation to layouts with larger segments with the same deck type and deck orientation, to provide options for more feasible construction. A third diaphragm layout is found with the traditional method for diaphragm design. All three designs for each diaphragm example are compared, and it is found that the freely optimized designs have the highest performance, followed by the interpreted design and the traditional designs are found not to be using the corrugated decks to their full potential. Future work remains: integration of gravity load constraints, incorporation of cost, non-linear behavior etc. Regardless of the future work ahead, this paper introduces the potential of topology optimization for rethinking the design of building diaphragms.

8. Acknowledgments

The authors gratefully acknowledge the financial support funded by the American Iron and Steel Institute, the American Institute of Steel Construction, the Steel Deck Institute, the Metal Building Manufacturers Association, the Steel Joist Institute and the US National Science Foundation through grant CMMI-1562821. Acknowledging the ideas and contributions collaborators in the Steel Diaphragm Innovation Initiative (SDII) have provided throughout the work on this paper. The authors also thank Krister Svanberg for providing the MMA optimizer code. Any opinions, findings, and conclusions or recommendations expressed in this material are those of the author(s) and do not necessarily reflect the views of the National Science Foundation or other sponsors.

References

[1] K. Svandberg, "The method of moving asymptotoes—a new method for structural optimization," Int. J. Numer. Methods Eng., 24, 359–373, 1987.

[2] S. Torabian, M. Eatherton, W. Easterling, J. Hajjar and B. Schafer, "SDII Building Archetype Design v1.0," CFSRC Report R-2017-04, 2017.

[3] M. Bendsøe and O. Sigmund, "Topology Optimization - Theory, Methods and Applications," Springer Verlag, 2002.

[4] T. Bruns and D. Tortorelli, "Topology optimization of non-linear elastic structures and compliant mechanisms," *Comput. Methods Appl. Mech. Engrg.,* pp. 3443-3459, 2001.

[5] J. Guest, J. Prevost and T. Belytschko, "Achieving minimum length scale in topology optimization using nodal design variables and projection functions," International Journal for Numerical Methods in Engineering, 61(2): 238 – 254, 2004.

[6] J. Guest and T. Igusa, "Structural optimization under uncertain loads and nodal locations," Computer Methods in Applied Mechanics and Engineering, 198(1), 116-124, 2008.

[7] AISI, "North American Standard for the Design of Profiled Steel Diaphragm Panels," S310, American Iron and Steel Institute, 2013.

[8] L. Luttrell, "Diaphragm Design Manual, fourth edition," Steel Deck Institute, 2015.

[9] Y. Xia and M. Friswell, "Equivalent Models of Corrugated Panels," International Journal of Solids and Structures, 49, 1453-1462, 2012.

[10] A. Fischer, J. Guest and B. Schafer, "Generation of Novel Building Diaphragm Layouts through Topology Optimization," Canadian Conference on Earthquake Engineering, Quebec, 2019.